Study of the interaction of folic acid-modified gold nanorods and fibrinogen through microfluidics: implications for protein adsorption, incorporation and viability of cancer cells

Received 00th January 20xx,
Accepted 00th January 20xx

DOI: 10.1039/x0xx00000x

Nacaroha Orellana,[a] Sujey Palma,[a,b] Estefania Torres,[a] María Luisa Cordero,[c] Valentina Vio,[b,d] Juan M. Ruso,[e] Josué Juárez,[f] Antonio Topete,[g] Marcelo J. Kogan,[b,d]* and Natalia Hassan[a,d]*

Gold nanoparticles (AuNPs) are an attractive nanomaterial for potential applications in therapy and diagnostic due to their capability to direct toward specific sites in the organism. However, when exposed to blood plasma, AuNPs can interact with different biomolecules that form a dynamic nano-bio interface called "protein corona" (PC). Remarkably, PC could affect multiple biological processes, such as cell targeting and uptake, cytotoxicity, and nanoparticle (NP) clearance. Previous works have widely studied these interactions in bulk conditions, which are distant from the dynamic scenario considering that different flow rates are present within the body that promotes several AuNP-biomolecule interactions. The interaction of nanomaterials with proteins has been widely studied in bulk conditions. However, the dynamic interaction of nanoparticles with proteins in dynamic conditions has just recently been explored. Thus, to mimic a dynamic natural environment, microfluidic devices were used. In this work, gold nanorods (GNRs) were synthesized and conjugated with two different modified polyethylene glycol (PEG), namely, HS-PEG-OMe and HS-PEG-COOH, to reduce their interaction with plasma proteins and increase their biocompatibility. Then, GNRs were functionalized with folic acid (FA) to recognize tumor cells. The nanosystem (GNR-PEG-FA) was exposed to fibrinogen (FB) to study the development and biological impact of PC formation. FB is one of the most abundant proteins in plasma, and considering their study behavior is possible through two strategies: bulk and flow conditions. The obtained nanosystems (GNR-PEG-FA/FB) were characterized by absorption spectrophotometry, dynamic light scattering (DLS), laser Doppler microelectrophoresis, and transmission electron microscopy (TEM). Finally, cell viability and cellular uptake assays were performed to study the influence of PC on the cytotoxicity and delivery of nanosystems.

Introduction

In the last years, the increase in the incidence of chronic diseases, such as cancer, diabetes, and cardiovascular conditions, associated with longer life expectancy in the Western world, has motivated the search for new platforms for more straightforward, faster, and more effective therapies and diagnoses[1].

Gold nanoparticles (AuNPs) are a developing alternative that has been studied for the treatment and diagnosis of multiple pathologies, including neurodegenerative disease, metabolic disorder, and cancer[2–7]. AuNPs present numerous advantages due to their nanometric size and are attractive because of their easily adjustable shape and size; biocompatibility; and their electronic, plasmonic, and photothermal properties. AuNPs can absorb energy from light. The absorb energy then dissipates as heat; this process is called photothermal effect. The absorb energy can be used for therapy to destroy toxic protein aggregates or malignant cells[8,9] or even for drug delivery applications[10]. Gold nanorods (GNRs), conversely, absorb light in the infrared region, which are also called the "biological window"; therefore, the absorption from biological molecules or tissues is minimal[11]. Previously, *in vivo* studies showed that applying infrared irradiation on GNRs produces selective destruction of tumor cells without any damage to the surrounding areas[12].

Furthermore, AuNPs have been used as drug delivery systems because of their high surface-to-volume ratio, which allows their surface functionalization with different ligands as drugs, tracers, or targeting molecules through a stable Au-S bound[13]. Different types of targeting molecules are employed to vectorized AuNPs toward the site of action in the organism and thus improve treatment effectiveness. In cancer, the AuNP surface is coated with molecules that have a high affinity for overexpressed receptors present in tumors or their

[a.] *Programa Institucional de Fomento a la I+D+I, Universidad Tecnológica Metropolitana, Ignacio Valdivieso 2409, San Joaquín.*
[b.] *Departamento de Química Farmacológica y Toxicológica, Facultad de Ciencias Químicas y Farmacéuticas, Laboratorio de Nanobiotecnología, Universidad de Chile, Santos Dumont 964, Independencia.*
[c.] *Departamento de Física, Facultad de Ciencias Físicas y Matemáticas, Universidad de Chile.*
[d.] *Advanced Center for Chronic Diseases (ACCDis). Santos Dumont 964, Independencia, Santiago, Chile.*
[e.] *Soft Matter and Molecular Biophysics Group, Department of Applied Physics,*
[f.] *University of Santiago de Compostela, Santiago de Compostela 15782, Spain.*
[g.] *Departamento de Física, Universidad de Sonora, Unidad Centro, Hermosillo, Sonora 83000, México*
[h.] *Laboratorio de Inmunología, Departamento de Fisiología, Centro Universitario de Ciencias de la Salud (CUCS), Universidad de Guadalajara, Guadalajara 44340, México.*
† E-mail: nhassan@utem.cl; mkogan@ciq.uchile.cl

Footnotes relating to the title and/or authors should appear here.
Electronic Supplementary Information (ESI) available: [details of any supplementary information available should be included here]. See DOI: 10.1039/x0xx00000x

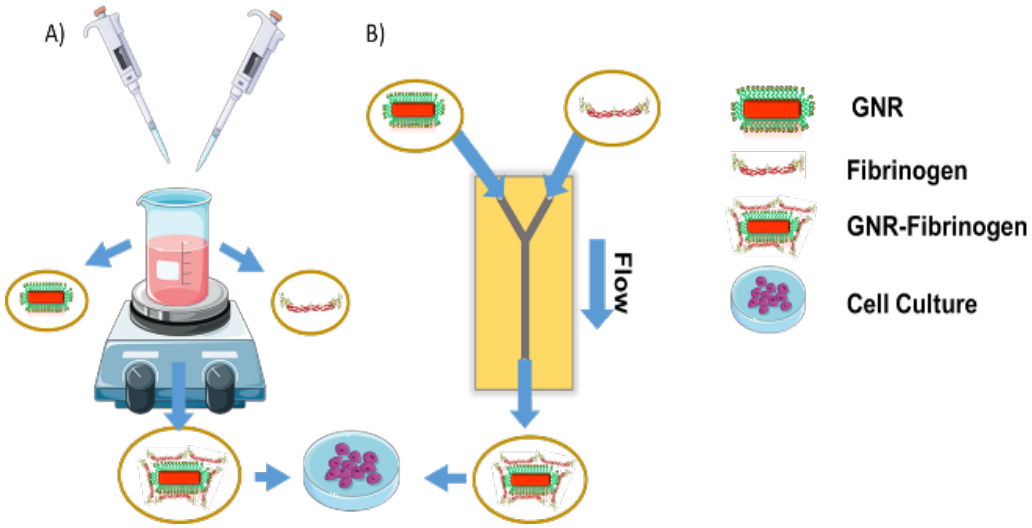

Scheme 1: Representation of the two experiments performed to study the GNR with FB. A) Bulk experiments; B) microfluidic experiments.

microenvironment[2]. For example, folate receptor (FRα) is highly overexpressed in tumor cells over normal tissues[14]. Therefore, folic acid (FA)-conjugated nanoparticles produce an improved selectivity toward tumor cells and increase cellular uptake through FRα-mediated endocytosis[15,16].

However, at the administration time, cell targeting, and uptake of NPs can be affected by the interaction with different biomolecules present in blood plasma, thus triggering a competition for the AuNP surface, forming the so-called "protein corona" (PC)[17–21]. Previous studies have shown that PC can affect several biological processes, such as nanoparticle uptake, biodistribution, cytotoxicity, transmembrane transport, hemolysis, and thrombocyte activation[22].

Plasma is a complex fluid that contains more than 3700 proteins, and at early times (<0.5 min), about 300 proteins can be found on the NP surface[22]. The composition of PC is heterogeneous and dynamic; and is influenced by protein concentration and the kinetic and equilibrium binding affinities (K_D) of each protein for specific NPs[20,23,24]. Therefore, studying the interaction between each protein and the specific nanoparticle is essential. Fibrinogen (FB) is one of the most abundant proteins in plasma and is essential for the formation of fibrin clots that prevent blood loss in case of vascular injury. Also, previous studies have shown that FB is a highly abundant species on AuNP surface[21] and promotes their phagocytosis and clearance via cells of the reticuloendothelial system (RES)[25–27].

Several works have been carried out to advance the knowledge regarding rates, affinities, and stoichiometric of the association of plasma proteins with AuNPs[23]. However, most of these interaction studies are *in vitro* models that fail to mimic the highly dynamic nature of blood and its heterogeneous flow velocity[28]. Conversely, *in vivo* strategies involve animal usage, which are limited by the cost and are time-consuming[19].

Microfluidics (MF) is a pioneering technique that offers the opportunity to analyze and study hydrodynamic regimes to generate new materials, order functionalization, or emulate dynamic enviroment[29]. Furthermore, MF allows to accelerate chemical reactions, permits the use few reagents, has lower costs, and reduces risks when handling reagents. Thus, MF has been widely used for chemical and biological applications, such as synthesis of nanoparticles, biosensors, and enzymatic reactors. To the best of our knowledge, MF has not been deeply used in the study of PC formation before, and only few works have reported this[30]. In addition, some authors propose the key role of rational NP design to specifically modulate the adsorbed or deflected proteins that can be a potentially powerful tool for nanomedicine. This knowledge could allow the control of NP delivery to specific sites in the body by manipulating factors that influence the PC[23]. For example, a widely used strategy to decrease PC formation is to attach polymers, such as polyethylene glycol (PEG), to the AuNP surface. The polymer acts as a barrier to decrease the interactions with plasma proteins, increase their circulation time, and confer stability[31]. Consequently, MF could be an inexpensive, quick, and animal-free alternative to the study of the interaction between NPs and PC and a rapid screening for new NP rational designs. In the present work, GNR coated with PEG and FA (GNR-PEG-FA) will be synthesized to direct toward tumor cells. Then, to simulate the dynamic environment in the organism, the GNR-PEG-FA will interact with FB (GNR-PEG-FA/FB) through two strategies: bulk and MF (Scheme 1). Furthermore, all nanosystems will be characterized by absorption spectrophotometry, dynamic light scattering (DLS), laser Doppler microelectrophoresis, and transmission electron microscopy (TEM). Finally, the effect of FB coating over the cell toxicity and uptake will be studied.

Results and discussion

First, GNRs were synthesized by a seed-mediated growth method, and to stabilize the GNRs, the GNR surface was covered with the cationic surfactant cetyltrimethylammonium bromide (CTAB; GNR-CTAB). Then, some CTAB molecules on the

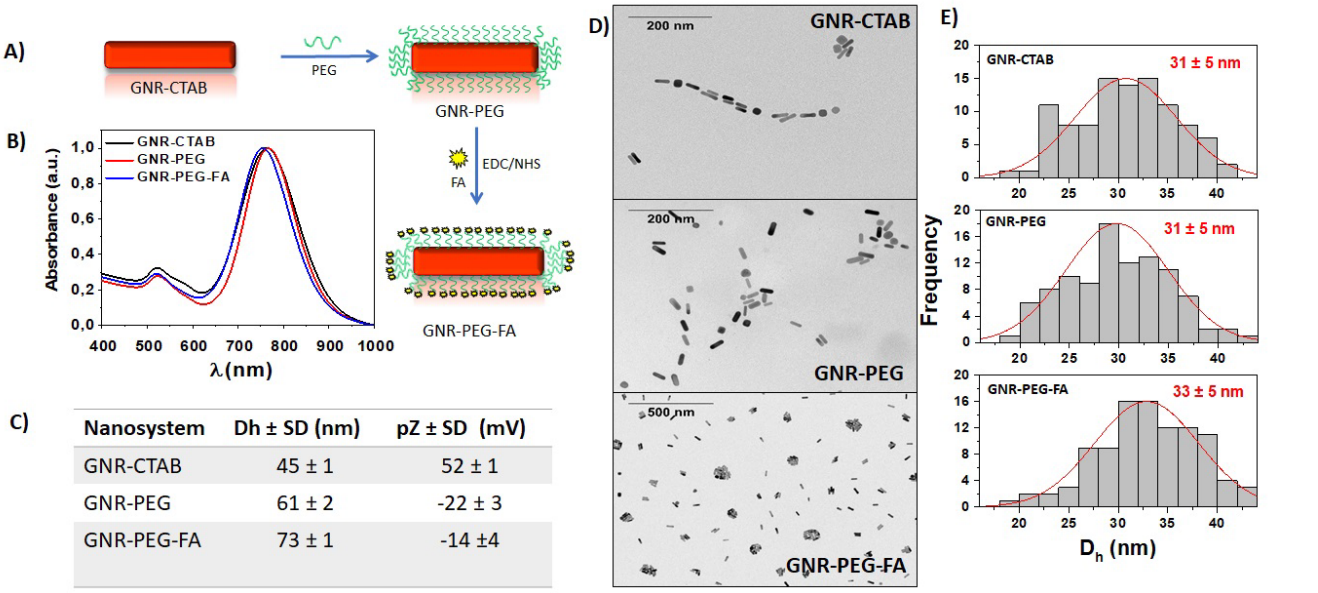

C)

Nanosystem	Dh ± SD (nm)	pZ ± SD (mV)
GNR-CTAB	45 ± 1	52 ± 1
GNR-PEG	61 ± 2	-22 ± 3
GNR-PEG-FA	73 ± 1	-14 ±4

Figure 1: Characterization of GNR-CTAB, GNR-PEG and GNR-FA obtained. A) Schematic representation of GNR functionalization with PEG and FA. B) UV-Vis absorbance spectrum, C) Table of hydrodynamic diameters values from DLS and Zeta potential of the nanosystems, D) TEM images and E) Histogram from TEM images of GNR-CTAB, GNR-PEG and GNR-FA.

Surface were replaced by PEG (GNR-PEG), which confers stability and biocompatibility, decreases interactions with plasma proteins, increases blood circulation time, decreases liver retention, and others[32–34]. Finally, GNR-PEG were functionalized with FA to selectively reach the tumor cells and increase cellular uptake. GNR conjugates were characterized through different techniques, such as absorption spectrophotometry, TEM, DLS and laser Doppler microelectrophoresis.

Figure 1-A shows a schematic representation of the GNR functionalization with PEG and FA. In addition, as seen in Figure 1-B, the absorption spectra of GNR-CTAB and their conjugates showed two characteristic peaks from transverse and longitudinal plasmon, as have been seen before in literature[35]. The transverse band at approximately 520 nm and a longitudinal one at approximately 750 nm that are in the so-called "biological window" (700–950 nm), where the biological tissues and molecules have their lowest absorption[11]. The absorption spectra of GNR-CTAB changed toward bathochromic regions when PEG and FA were added to the GNR surface, from 755 to 768 nm.

Then, DLS and laser Doppler microelectrophoresis measurements confirmed the functionalization of the GNR-CTAB surface due to changes in the hydrodynamic diameter (D_h) and Zeta potential (pZ) as displayed in the table in Figure 1-C. The results show that the longitudinal D_h of the GNR-CTAB increases from 45 ± 1 nm to 61 ± 2 nm due to PEG adsorption onto the GNR-CTAB surface through chemisorption of thiol-Au bond giving the GNR-PEG system. Then, GNR-PEG were functionalized with FA through an amide bond with the carboxylic group from PEG, resulting in a nanosystem of 73 ± 1 nm. These results demonstrated the correct functionalization of GNR-CTAB by the increase in size. Additionally, pZ changes from positive to negative values, indicating that the GNRs were functionalized. First, GNR-CTAB presents a positive pZ of 52 ± 1 mV because of the presence of cationic surfactant molecules on the GNR surface that provides stability. Then, after PEG conjugation, the pZ diminished to negative values, −22 ± 3 mV, due to the carboxyl groups from PEG, which are deprotonated at pH 7.4. Finally, the functionalization with FA changes the surface charge slightly to −14 ± 4 mV, which can be explained by the following: the FA molecules have two carboxyl groups; however, only one of them is deprotonated at pH 7.0 to form COO- at pH 7 (γ-carboxylic acid group) (FA pKa1 = 2.3, pKa2 = 8.3)[36]. Therefore, the nanosystem charge is practically similar[37].

Figure 1-D displays TEM images of GNR-CTAB, GNR-PEG, and GNR-PEG-FA, in which their shape and size are shown and revealed an aspect ratio (length/width) of about 4. Also, histograms (Figure 1-E) exhibit the distribution of length of the nanosystems where the average length of the GNR-CTAB, GNR-PEG, and GNR-PEG-FA is 31 ± 5, 31 ± 5, and 33 ± 5 nm, respectively.

Then, to study the interactions between GNR-PEG-FA and the plasmatic protein FB, bulk method was used, specifically magnetic stirring at room temperature (RT). Different incubation times (10, 30, and 60 min) were tested in the bulk method, and the resulted nanosystems (GNR-PEG-FA/FB, which will be assigned as GNR-FB for simplicity) were separated by centrifugation from the free protein and were also characterized through the technique mentioned above.

Figure 2-A displays the absorption spectra of GNR-FB from different incubation times. Previous studies have determined that the plasmon resonance depends on particle size moving toward longer wavelengths as size increases[9]. In this case, there are no significant displacements along with spectrum bands because the FB does not have a considerable effect on the refractive index of the GNRs. As shown in Figure 2-B (table), the D_h values from all the GNR-FB systems increase due to the PC

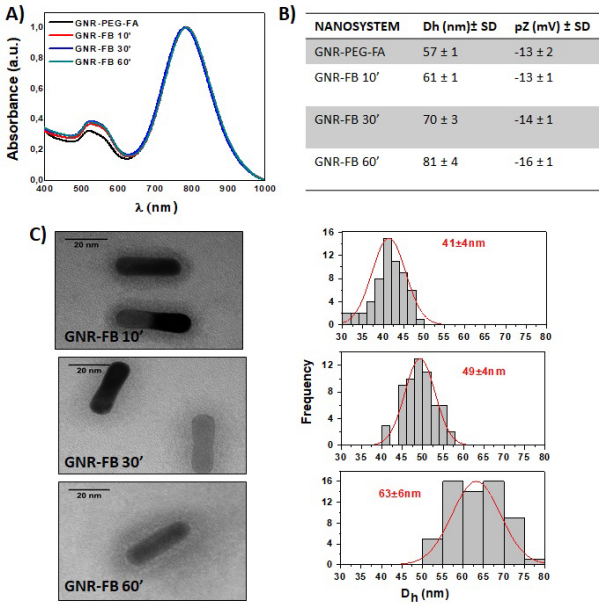

Figure 2: Characterization of GNR functionalized. A) UV-Vis absorbance spectrum. B) Table of Dh obtained by DLS (Dh, nm) and pZ (mV) of GNR-PEG-FA, GNR-FB 10', GNR-FB 30' and GNR-FB 60'. C) TEM images of GNR-FB at different time of interaction. D) Histograms of TEM images.

formation around the nanoparticle surface, and this increment is proportional to the incubation time. Previous works showed that AuNP-protein interaction depends on the presence of thiol groups in the protein structure and on their electrostatic properties[38,39]. The FB structure presents 11 cysteine residues on its surface with thiol groups to form a stable S-Au bond with the AuNPs; thus, FB has a higher binding affinity (K_D) than the other plasma proteins[20]. Nevertheless, polymers can be grafted to the gold surface at high densities, and in this scenario, the polymers adopt a brushlike configuration and proteins interact primarily with the terminal groups of the polymers chains[40]. On the other hand, pZ did not reveal significant changes in the GNR-PEG-FA surface charge at different interaction times. These results can be explained by the fact that FB has an isoelectric point at pH 5.8 and is therefore negatively charged at pH 7.4. Additionally, GNR-PEG-FA and FB have a net negative charge, where FB provides a protecting effect that reduces the overall negative nanoparticle surface charge. Also, this protective shell consequently reduces the nonspecific electrostatic repulsion between the surface and protein in solution, enhancing the binding of the subsequent FB molecules[40].

Therefore, the negative charge of GNR-PEG-FA is maintained.

As illustrated in Figure 2-C, GNR-FB at different incubation times are not agglomerated and maintain the same rod shape; however, it also shows a clear FB coating on their surface due to the prior staining of the organic material. Also, the histogram obtained from TEM images demonstrates how the GNR-PEG-FA size increases with the time of interaction between FB and the nanosystem. In a previous work, Dobrovolskaia et al. used TEM images to confirm NP size and avoid the subsequent DLS measurements of NP agglomerates[21].

Later, microdevices were fabricated to evaluate the interaction between GNR-PEG-FA and FB under dynamic conditions. Microchips were made with polydimethylsiloxane (PDMS) using two different geometries, which are called the Y- and S-shape; both are represented in Figure 3. The two selected geometries were used to compare the residence time (t_R) between both and the interaction between NPs and FB. In both geometries, two inlet channels converge into one long outlet channel, and in S-shape, the outlet is bent in several curves to increase the t_R of the GNRs in the microchannel. GNR-PEG-FA and FB were injected through each inlet channels. FB flow rate (Q) remains constant at 2 mL/h, while GNR-PEG-FA flow varies at different flow rates: Q_1 = 2 mL/h, Q_2 = 1.5 mL/h, and Q_3 = 1 mL/h. The samples were collected and then analyzed by the techniques mentioned above. In order to ensure that effectively the flow is laminar throughout the device we have performed computational fluid dynamics as we have previously described. Considering the fluid model predictions, in **Figure ……** we show the determined velocity field gradients for an input velocity of 2 ml/h (the highest input velocity in this study). Consequently, these results show that laminar flow is present through all the geometry and velocities, which is expected considering the Reynolds numbers. Although in relatively simple cases the characteristics can be predicted, thus it is very easy to modify this profile, varying the speeds, and the efficiency of the mixing according to our needs. However, in this case, the only means by which molecules in different fluxes can be mixed is dependent upon individual molecular diffusion through the interface between the fluid streams.

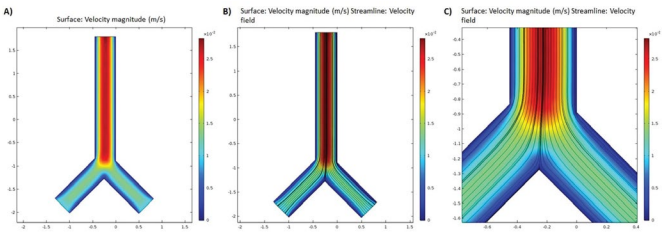

Figure 3. Velocity countour planes and streamlines for the whole device (A), first Y-junction (B) and second Y-junction (C).

The flow rates have influence in the interaction with GNR. Figure 4 displays the absorption spectra from the resulted complex GNR-FB by MF at Q_1, Q_2, and Q_3 regimes. For the Y-shape conformation, it was observed that the plasmonic band of the GNR-PEG-FA has a bathochromic displacement at Q_2 and Q_3, which change from 745 to 794 nm (Figure 4-A). Also, similar results were obtained with the S-shape conformation, where, at Q_3, the slower flow, redshift from 747 to 794 nm, was observed. The reason for this can be that, at these flows, nanoparticles interact much longer with the protein because the flow rates are is slower, giving the possibility that the protein keeps contact with the nanoparticles in a longer time, adding more protein at its surface. Thus, the nanoparticle size increases, and therefore, the absorbance peak changes to the near-infrared region.

Perturbation response maps based on elastic network models (ENM) have been extensively reported to study relevant conformational changes of several proteins at the atomistic and molecular level. Because, it is well-known that the first elastic normal modes could describe a large number of different conformational states of the protein. In this regard, one of the most important steps is the determination of the degree of collectivity of the system evaluated (González-Durruthy, M., Scanavachi, G., Rial, R., Liu, Z., Cordeiro, M. N. D., Itri, R., Ruso, J. M. (2019). Structural and energetic evolution of fibrinogen toward to the betablocker interactions. *International journal of biological macromolecules*, *137*, 405-419). The degree of collectivity (K_k) of a given mode (k) determines the collective protein motions like an extent to which the structural elements (block of consecutive residues) move together in a given conformational mode. Then, a high degree of collectivity ($K_k \approx 1$) represents a highly cooperative conformational changes strictly dependent on the low-frequency normal modes (k) that exhibit larger amplitudes of correlated motions for a large number of C-(α) atoms affecting partially or the whole structure describing global rotations-translations of consecutive residue blocks by conformational anisotropic movements. While, high-frequency modes exhibit small amplitude and localized motions (as bending and bond stretching) which are usually associated with low collectivity (González-Durruthy, M., Scanavachi, G., Rial, R., Liu, Z., Cordeiro, M. N. D., Itri, R., Ruso, J. M. (2020). Mapping the underlying mechanisms of fibrinogen benzothiazole drug interactions using computational and experimental approaches. *International Journal of Biological Macromolecules*,*163*, 730-744.). Figure .... (puedes escoger alguna de las jmol) shows a scheme of the movements (elasticity) of the fibrinogen obtained from the lowest normal mode (the most probable). As can be seen this mode exhibit the highest collectivity involving all the domains of the fibrinogen (the cross correlation matrix can be consulted in the supporting information). This is, despite maintaining the original structure intact, the fibrinogen molecule, under normal conditions, presents some flexibility. The probability of the modes of vibration can be altered by changing the conditions of the environment, thus changing the flexibility of the protein. Obviously, changes in flow rates fall into this category by modifing the flexibility of the protein and consequently its interaction with the nanoparticles.

Thus, the combination of longer contact times with diverse flexibilities of the proteins results in the different patterns of interactions observed

Figure 4-C shows the D_h and pZ of all the GNR-FB by dynamic conditions. D_h increases as the flow rates of the nanoparticles

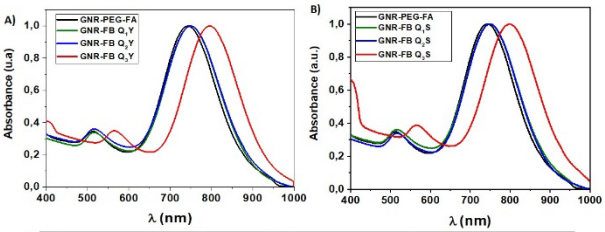

C)

Y-shape	Dh ± SD (nm)	pZ ± SD (mV)	S-shape	Dh ± SD (nm)	pZ ± SD (mV)
GNR-FB Q_1Y	56,7 ± 2	-20 ± 1	GNR-FB Q_1S	77,2 ± 2	-16 ± 1
GNR-FB Q_2Y	70,1 ± 1	-24 ± 5	GNR-FB Q_2S	83,8 ± 1	-21 ± 3
GNR-FB Q_3Y	89,9 ± 2	-25 ± 2	GNR-FB Q_3S	89,7 ± 1	-22 ± 2

Figure 4: UV-Vis spectra of nanosystems obtained by microfluidics. A) Nanosystem from Y-shape microchip. B) Nanosystem from S-shape microchip. C) Table of hydrodynamic diameters (Dh) and Z potential from Y-shape and S-shape experiments.

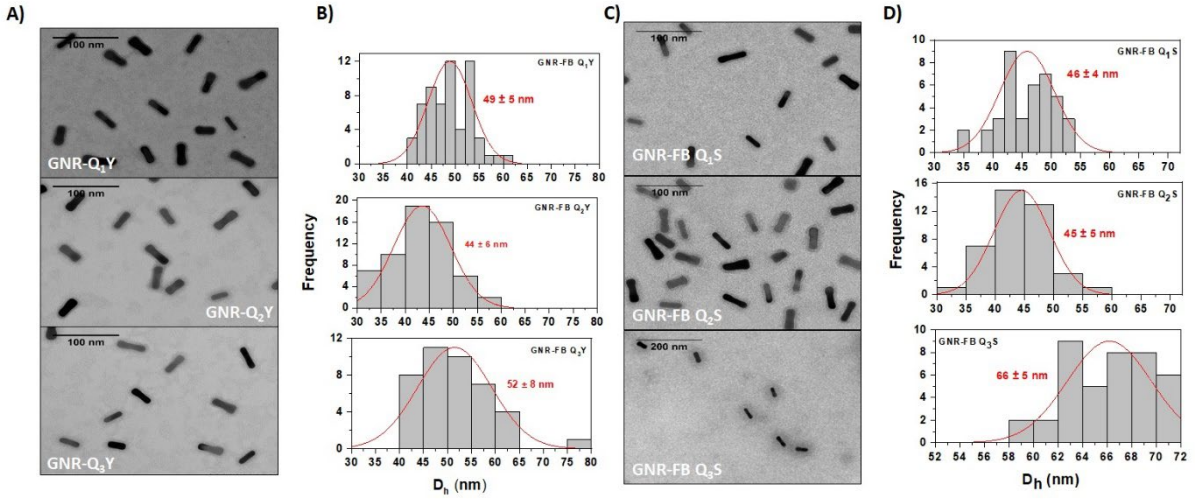

Figure 5: Micrographs with their respective particle diameter histogram (A) TEM images of GNR-FA Q_1Y, Q_2Y, Q_3Y, (B) Histogram of A. C) TEM images of GNR-FA Q_1S, Q_2S and Q_3S. D) Histogram of C.

decrease. As was explained above, this could be due to the fact that the protein interacts for a longer time with the nanoparticle, increasing the number of proteins added to the GNR surface (Figure S-1 to S-12, Supporting Information). The absolute value of pZ increases to negative values as the flow rates of the nanoparticles decreased. However, no significant changes were obtained, owing to that fact that, since FB is absorbed onto the nanoparticle surface, the negative charge of the nanosystem remains with the addition of more protein.

Furthermore, TEM images in Figure 5 show the size and shape of the nanosystems. Rod shape and no agglomerates of the GNR-FB were observed, indicating the correct coverage of the nanoparticles. Also, the micrographs exhibit the PC formed around the GNR surface, which varies according to the different GNR-PEG-FA flow rates. In the case of the nanosystems from Y-shape conformation, an increase in nanoparticle size was observed (Figure 5-A and 5-B). Nevertheless, for S-shape conformation, Q_3 has the major increase in size in comparison to Q_2 and Q_1 (Figure 5-C and 5-D).

To evaluate the influence of PC over the effect on cell viability of the GNRs and their conjugates, viability assays were performed in HeLa cells. First, GNR-CTAB, GNR-PEG, and GNR-PEG-FA were assessed at different concentrations (0.25, 0.5, 0.75, and 1 nM) to determine the influence of CTAB displacement in the cytotoxicity potential. Then, GNR-FB obtained from bulk and MF was used at a fixed concentration of 0.25 nM to simplify the results. All the experiments were performed for 24 hours, and the cells were maintained at 37°C and 5% pCO_2. Live and death controls were performed with supplemented medium and 10% sodium dodecyl sulfate (SDS), respectively.

Also, vehicle controls were made with sterile water for GNR-CTAB and GNR-PEG, while 50 mM glycine buffer at pH 8.5 for GNR-PEG-FA and GNR-FB, as this buffer is necessary to resuspend FB. As illustrated in Figure 6, GNR-CTAB is toxic for all the evaluated concentrations. Previous studies have shown that GNR-CTAB have toxic effect over the cells[41]. Then, GNR-PEG presents lower cell viability effects, which is inversely proportional to their concentration (Figure 7-A). GNR-PEG-FA does not show any significant cytotoxic effect in HeLa cells for the given range of concentration (Figure 7-B). These findings correspond with previous studies in which the CTAB displacement from the GNR-CTAB surface allows lower effects on cell viability[42]. Regarding the complex GNR-FB display in Figure 7-C and Figure 7-D, it did not reveal cytotoxic effects in HeLa cells under all the tested conditions. These findings are explained by the fact that there are no significant differences between cell viability from this complex and the live control. Also, this behavior is consistent with previous reports in which other proteins, as apolipoproteins, confer a diminution in the effect on cell viability character to the drug delivery systems[23].

Finally, HeLa cells express FRα that allows the internalization of drug delivery systems linked to FA by receptor-mediated endocytosis[43]. To assess the influence of FB over the GNR-PEG-FA internalization process, HeLa cells were incubated with GNR-PEG-FA and GNR-FB from bulk and dynamic conditions for 24 hours. Later, gold amount in cells was quantified by neutron activation analysis (NAA).

As shown in Figure 8-A and Figure 8-B, the micrograms of gold incorporated in HeLa cells are 0.06 μg for GNR-PEG-FA in comparison with GNR-FB nanosystems. The PC formation by MF

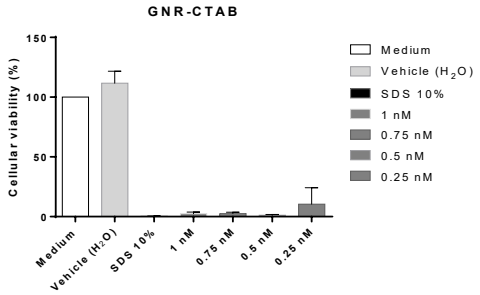

Figure 6: Evaluation of the cytotoxicity of different concentrations of GNR-CTAB in the HeLa cell line through

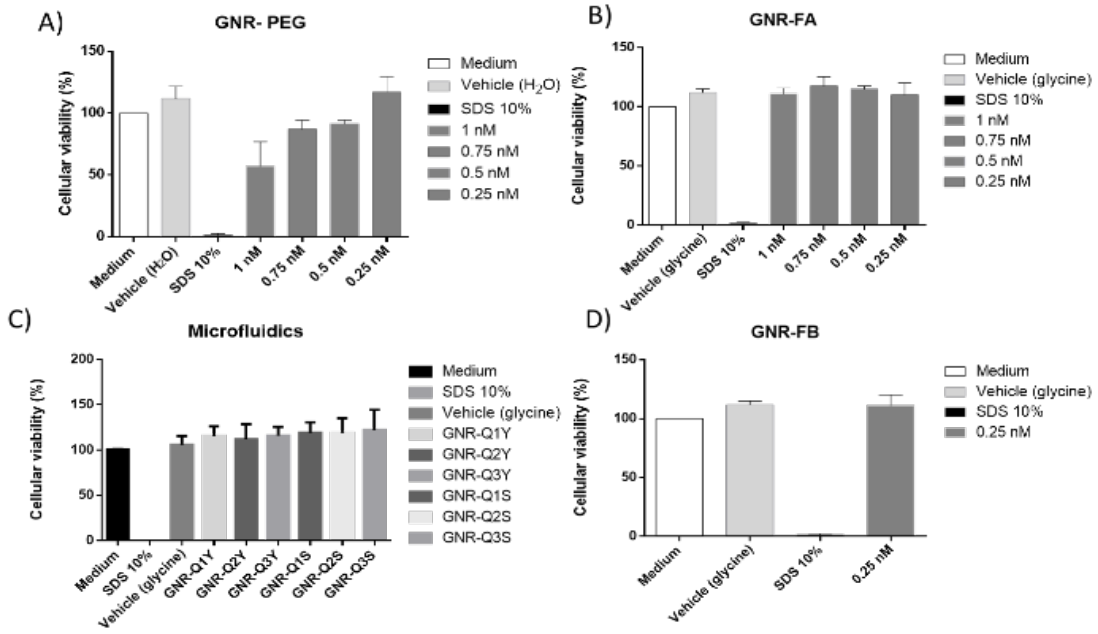

Figure 7. Cell viability test in the HeLa cell line.

and bulk was different in both experiments. In the bulk method, the micrograms of gold for GNR-FB 10', GNR-FB 30', and GNR-FB 60' were 0,014 ± 0,0013, 0,020 ± 0,0004, and 0,022 ± 0,0015 μg, respectively; nevertheless, for MF experiments, these values diminished considerably. These results indicate that the interaction with FB in bulk or fluid conditions could be different, provoking a different interaction with cells. Thus, it can be hypothesized that the PC formation in bulk or fluid conditions could be different.

Predicting *in vivo* behavior with the use of *in vitro* models is still in its infancy. It is already known that nanoparticles can be evaluated using *in vitro* cells in cultured cell plates, which does not resemble the complexity of *in vivo* nanoparticle-cell interaction. Within a well plate, results could confound final interpretations, increasing the errors in the conclusion of the experiments. For this reason, MF has several advantages over conventional methods for cell and protein interactions through the incorporation of fluid flow and mechanical forces, bringing a step closer to mimicking the *in vivo* microenvironment. In this sense, MF can emulate a real environment to study the nanoparticle-protein interaction by simulating a PC formation in the bloodstream. In previous studies, it was demonstrated that the existence of shear flow induces the conformational transitions of some proteins. Kroll et al. demonstrated that shear flow induces a change in the quaternary structure of the whole multi-unit chain of Von Willebrand factor from a compact globular state to the elongated fiber-like conformation. This plasma protein and platelets work together in the hemostasis process, and the fact that hydrodynamic forces induce conformational transitions may provide a basis for a self-regulatory repair mechanism of blood vessel wall (ref). Another example is the work by Loksztejn and Dzwolak who studied insulin fibrillation by hydrodynamic forces, demonstrating that these forces induce insulin aggregation and subsequent formation of chiral amyloid structures (ref). Lee et al. studied amyloid formation in a microfluidic device, analyzing the influence of the flow rate on the kinetics of the process (ref). In the present work, the possible utility of microfluidic technology was demonstrated to study protein-nanoparticle interaction within a microchannel, which could be extrapolated for the study of nanoparticle interactions in a hydrodynamic state, an approach closer to reality.

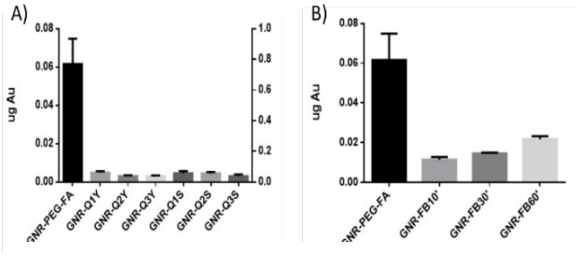

Figure 8: Gold content profiles in HeLa cells that were treated with different interactions by microfluidics (A) and bulk (B).

Experimental

Materials and methods

Materials. For the GNR synthesis, gold (III) chloride hydrate (HAuCl4), CTAB, sodium borohydride (NaBH4), L-ascorbic acid, silver nitrate ($AgNO_3$), 1-ethyl-3-(3-dimethylaminopropyl) carbodiimide (EDC) and N-hydroxysuccinimide (sulfo-NHS), FA, phosphate buffered saline (PBS), and MES (2-(N-morpholino)ethanesulfonic acid) buffer were purchased from Sigma-Aldrich (MO, USA). HS-PEG-OMe and HS-PEG-COOH MW 5000 Da were obtained from JenKem Technology (TX, USA). Milli-Q water was used in all experiments.

For cell experiments, HeLa cells were supplied by ATCC (VA, USA). Dulbecco's Modified Eagle Medium (DMEM), penicillin, and streptomycin were purchased from GIBCO, Thermo Fisher (MA, USA), and fetal bovine serum (FBS) was obtained from HyClone™ (USA). MTS assay kit was purchased from Promega (WI, USA).

For microdevice fabrication, PDMS and SYLGARD™ 184 were supplied by Dow Corning (MI, USA), and SU-8 photoresist (GM1075) was obtained from Gersteltec (Pully, Switzerland).

Synthesis of gold nanorods. GNRs were synthesized using a seed-mediated growth method[10,44]. All glassware material was previously washed with aqua regia and subsequently rinsed and dried to eliminate any metal contamination. First, seed solution was prepared by reducing 42.5 µL of $HAuCl_4$ (29.4 mM) in a solution of 4.7 mL of CTAB (0.1 M) with 300 µL of a cold solution of $NaBH_4$ (10 mM) under agitation conditions at 27°C. Separately, a growth solution was prepared consisting in 170 µL of $HAuCl_4$ (29.4 mM) in 10 mL of CTAB (0.1 M). Later, 75 µL of L-ascorbic acid (0.1 M) and 80 µL of $AgNO_3$ (5 mM) were added under gentle agitation at 27°C. Then, 120 µL of seed solution was added into the growth solution with a vigorous agitation at 27°C. This solution reacted for 30 minutes at 27°C to obtain GNR-CTAB. Finally, the GNR-CTAB were centrifuged at 7030 g for 30 minutes, and the *pellet* was resuspended in Milli-Q water.

GNR-CTAB functionalization. To functionalize the GNR-CTAB with FA, GNR-CTAB were conjugated with HS-PEG-OMe and HS-PEG-COOH (MW, 5000); then, FA was attached to GNRs via EDC/NHS coupling reaction. First, 50 µL of HS-PEG-OMe (1 nM) solution was added to 9.9 mL of GNR-CTAB to pH 12 with magnetic stirring for 10 minutes at RT to obtain GNR-PEG-OMe. Then, the mixture was centrifuged at 7030 g for 10 minutes to discard the excess of SH-PEG-OMe, and the pellet was resuspended in 10 mL of Milli-Q water; the pH was adjusted at 12. Subsequently, 300 µL of HS-PEG-COOH (1 nM) solution was added to GNR-PEG-OMe solution; then, it was incubated under stirring for 1 hour at RT to obtain GNR-PEG-COOH. Then, the mixture was sonicated for 10 minutes and centrifuged at 7030 g for 10 minutes. Later, to perform the FA conjugation, the resulted pellet was resuspended in a mixture of 0.2 mg of EDC and 0.5 mg of sulfo-NHS in 100 µL of MES buffer solution (0.1 M) to pH 5.5 and sonicated for 15 minutes. The mixture was centrifuged at the same mentioned conditions, and the pellet was mixed with 0.5 mg of FA in 500 µL of PBS buffer at pH 7.4 and incubated overnight at RT. The obtained GNR-PEG-FA solution was then centrifuged again to eliminate FA-free molecules.

Gold nanorod characterization. UV-visible spectrophotometry was used to determine the surface plasmon band of GNR-CTAB and its conjugates. UV-visible absorption spectra were recorded at RT with Perkin Elmer spectrophotometer model Lambda 25 UV. The different GNR samples were measured in disposable cells at a dilution of 1:20 in Milli-Q water. The measurement was performed in the wavelength range of 400–1000 nm, and Milli-Q water was used as blank. Also, to determine the D_h, DLS was used, while the surface charge was measured by laser Doppler microelectrophoresis. Both parameters were measured through Malvern ZetaSizer Nano ZS equipment. For this purpose, a 1:20 dilution of each nanosystem was performed using Milli-Q water. Each sample was placed in a disposable capillary cell and measured for a minimum of three times per sample. The results are expressed in terms of D_h (nm ± SD) and pZ (mV ± SD). Finally, to determine the size and morphology of nanoparticles, TEM was performed. The samples were deposited on copper grids with a Formvar/carbon membrane for 10 minutes and then stained with phosphotungstic acid to stain the organic material. The supernatant was then removed, and grids were left to dry before observation through TEM using a Hitachi HT7700 electron microscope. Finally, particles were measured by ImageJ software, and the data were represented as histograms as the number of GNR vs. length.

Microchip fabrication. Microdevices were fabricated with PDMS from masters made of SU-8 GM1075 photoresist using an optical lithography technique. Two geometry designs were used, as shown in Figure 3 (which is called the Y- and S-shape). Both microdevices present two inlet channels that converge into one outlet channel. Still, S-shape presents several curves through its outlet channel to increase the t_R of the NPs and FB. The width and height of the channels are 500 and 200 µm, respectively.

Description of the numerical solution applied to fluid flow. To further characterize the profile of the velocity field inside the microfluidic device, a 2D model of the system was created using COMSOL Multiphysics 4.3. From this model a mesh file was created, and finite volume method was applied to solve the associated differential equations that govern the fluid phase, in this case, the incompressible Navier-Stokes equations:

$$\nabla \cdot u = 0$$
$$-\nabla\eta(\nabla u + (\nabla u)T) + \rho u \cdot \nabla u + \nabla \mathrm{p} = 0$$
$$-\nabla(-D\nabla \mathrm{c} + cu) = 0$$

Being η, u, ρ the dynamic viscosity, velocity and pressure. D and c are the mutual diffusivity and the concentrations of the steams, respectively. The computational method was utilized to predict the velocity profiles of flow through the channels, contours of shear stress over the chorion surface and concentration of over time. Besides, the reagents were incompressible liquids, the mixture was suitable for simulating and the phases were treated as interpenetrating continua. Finally, the boundary condition for the inner walls of the channels was assumed as no-slip condition as well as zero diffusional flux at the wall of the channel.

Interaction of GNR-PEG-FA with fibrinogen. The interaction between GNR-PEG-FA and FB protein was evaluated by two strategies: bulk and dynamic conditions. For bulk conditions, 500 µL of GNR-PEG-FA concentration were incubated with FB concentration with a gentle agitation for 10, 30, and 60 minutes at 4°C. Then, the samples were centrifuged at 7030 g for 10 minutes to discard the free FB. On the other hand, the dynamic

conditions were performed through the use of microdevices. GNR-PEG-FA and FB concentrations were separately injected through each inlet channel. Q remains constant at 2 mL/h, while GNR-PEG-FA flow varies at different flow rates: Q_1 = 2 mL/h, Q_2 = 1.5 mL/h, and Q_3 = 1 mL/h. Flow rates were controlled by the injection pumps Genie Touch and K_D Scientific that allow standardizing the rates according to the syringe. Samples were collected at the end of the outlet channel and centrifuged at 7030 g for 10 minutes to discard the free FB. Finally, samples from the static and dynamic conditions were characterized through UV-visible spectrophotometry, DLS, laser Doppler microelectrophoresis, and TEM.

Perturbation response maps and collectivity degree-based elastic network models. This computational approach evaluates the degree of change in the residues network of fibrinogen by describing the potential (*U*) as a Hookean potential based on an elastic network analysis (ENM). Herein, the perturbation response was estimated by averaging across all the fibrinogen residues for different amplitudes from equilibrium using anisotropic vibrational analysis. The perturbation response is depicted as a local perturbation response scanning map (LPRS map). Here the i^{th} rows are related to the response generated upon perturbing fibrinogen residue (*i*) and its average (*i.e.*, over all *k*-receivers residues of fibrinogen). While the k^{th} columns of the LPRS maps depict the sensitivity in response to the perturbation for all the fibrinogen allosteric residues (*j*-sensors residues) . We also consider other recognized parameters, like the degree of collectivity (*K*) for a given *k*-normal mode. This biophysical parameter informs about how the structural elements (fibrinogen residues) move together in that particular mode, this is the cooperativity degree (López-Blanco JR, Garzón JI, Chacón P. (2011) iMod: multipurpose normal mode analysis in internal coordinates. Bioinformatics. 27 (20): 2843-2850) (Kovacs J., P. Chacón, R. Abagyan. (2004) Predictions of Protein Flexibility: First Order Measures. PROTEINS: Structure, Function, and Bioinformatics. Proteins. 56(4):661-8).

Cell culture. HeLa cells were cultured in T75 culture flasks in DMEM supplemented with 10% of FBS and maintained in a humidified incubator at 37°C and 5% pCO2. Media were changed every 2 days, and cells were detached using 0.25% trypsin.

Cell viability assay. GNR cytotoxicity was evaluated by MTS assay. Formazan is the product from the reduction of 3- [4,5-dimethylthiazol-2-yl] -5- [3-carboxymethoxyphenyl] -2- [4-sulfophenyl] -2H-tetrazolium (MTS) in the presence of PMS, which indicate cell viability. Then, 10,000 HeLa cells were plated in a 96-well multiplate with DMEM/F12 supplemented with 1% FBS. GNR-CTAB, GNR-PEG, and GNR-PEG-FA were assessed at 0.1, 0.25, 0.5, and 0.75 nM. GNR-FA/FB from bulk (de cual tiempo de incubación?) and dynamic conditions were evaluated at 0.25 nM. The test was performed for 24 hours since the treatment was added, and the cells were maintained at 37°C and 5% pCO_2. Also, live, death, and vehicle controls were performed with supplemented medium, 10% SDS, and glycine buffer 50 mM at pH 8.5, respectively. Then, the medium was discarded and cells were incubated with 80 µL of colorless DMEM/F12 and 20 µL of MTS/PMS solution for 1 hour at 37°C and 5% pCO_2. Measurements were performed at 490 and 655 nm in BioTek Synergy™ Mx Microplate Reader. All these experiments were performed three times.

Cellular incorporation assays. The amount of gold into HeLa cells was determined by NAA, to assess the influence of the FB corona in the GNR-PEG-FA cell internalization; 60,000 HeLa cells were seeded in 24-well multiplate and were incubated with GNR-PEG-FA (0.5 nM) and GNR-PEG-FA/FIB (0.5 nM) from the static and dynamic experiments for 6 hours at 37°C and 5% pCO_2. Also, a control was performed with a supplemented medium. Then, cells were washed five times with PBS buffer at pH 7.4 to eliminate the GNRs that did not interact with HeLa cells. Subsequently, cells were detached, and the gold amount was quantified by NAA.

Conclusions

When AuNPs interact with plasma proteins, these proteins can coat the nanoparticle surface, forming the PC. Previous studies confirmed that PC can affect the physical properties and several biological processes of the nanoparticles, such as cellular uptake, biodistribution, cytotoxicity, and clearance. In this work, GNR-PEG-FA were successfully synthetized by a growth seed-mediated method and functionalized with PEG and FA to improve their cell uptake by tumor cells. The interaction between GNR-PEG-FA and FB through bulk conditions showed changes in their absorption spectra, TEM images, and D_h. Microdevices with different geometrical conformations were fabricated using optical lithography techniques. GNR-FB obtained by MF demonstrates that, at slower flow rate, more proteins are added to the surface of nanoparticles, indicating the importance of the time of interaction in dynamic conditions. Viability assays revealed that FB corona on the GNR-PEG-FA surface did not affect their biocompatibility in HeLa cells. Internalization studies showed that the FB coating significantly decreases the cellular uptake of GNR-PEG-FA in HeLa cells in comparison with bulk experiments. Finally, MF could be a reliable, simple, and cheap tool for the study of the NP-protein interactions and even for the subsequent evaluation of new strategies that modulate the NP-protein interaction, thus allowing a rational design of nanoparticles.

Conflicts of interest

There are no conflicts of interest to declare.

Acknowledgments

Natalia Hassan acknowledges to the FONDECYT de Iniciación N°11170849, FONDAP 15130011 and project REDI170258.

Notes

There are no notes to incorporate.

References

1. de Morais MG, Martins VG, Steffens D, Pranke P, da Costa JAV. Biological applications of nanobiotechnology. *J Nanosci Nanotechnol*. 2014;14(1):1007-1017. doi:10.1166/jnn.2014.8748
2. Lopes TS, Alves GG, Pereira MR, Granjeiro JM, Leite PEC. Advances and potential application of gold nanoparticles in nanomedicine. *J Cell Biochem*. 2019;120(10):16370-16378.
3. Aghaie T, Jazayeri MH, Manian M, et al. Gold nanoparticle and polyethylene glycol in neural regeneration in the treatment of neurodegenerative diseases. *J Cell Biochem*. 2019;120(3):2749-2755.
4. Baranes K, Shevach M, Shefi O, Dvir T. Gold Nanoparticle-Decorated Scaffolds Promote Neuronal Differentiation and Maturation. *Nano Lett*. 2016;16(5):2916-2920. doi:10.1021/acs.nanolett.5b04033
5. Muller AP, Ferreira GK, Pires AJ, et al. Gold nanoparticles prevent cognitive deficits, oxidative stress and inflammation in a rat model of sporadic dementia of Alzheimer's type. *Mater Sci Eng C Mater Biol Appl*. 2017;77:476-483. doi:10.1016/j.msec.2017.03.283
6. Chen H, Ng JPM, Bishop DP, Milthorpe BK, Valenzuela SM. Gold nanoparticles as cell regulators: beneficial effects of gold nanoparticles on the metabolic profile of mice with pre-existing obesity. *J Nanobiotechnology*. 2018;16(1):88. doi:10.1186/s12951-018-0414-6
7. Qiu W, Chen R, Chen X, et al. Oridonin-loaded and GPC1-targeted gold nanoparticles for multimodal imaging and therapy in pancreatic cancer. *Int J Nanomedicine*. 2018;13:6809-6827. doi:10.2147/IJN.S177993
8. Stefani M, Dobson CM. Protein aggregation and aggregate toxicity: new insights into protein folding, misfolding diseases and biological evolution. *J Mol Med (Berl)*. 2003;81(11):678-699. doi:10.1007/s00109-003-0464-5
9. Berry CC, Curtis ASG. Functionalisation of magnetic nanoparticles for applications in biomedicine. *J Phys D Appl Phys*. 2003;36(13):R198-R206. doi:10.1088/0022-3727/36/13/203
10. Morales-Zavala F, Arriagada H, Hassan N, et al. Peptide multifunctionalized gold nanorods decrease toxicity of β-amyloid peptide in a Caenorhabditis elegans model of Alzheimer's disease. *Nanomedicine Nanotechnology, Biol Med*. 2017;13(7):2341-2350. doi:10.1016/j.nano.2017.06.013
11. Adura C, Guerrero S, Salas E, et al. Stable conjugates of peptides with gold nanorods for biomedical applications with reduced effects on cell viability. *ACS Appl Mater Interfaces*. 2013;5(10):4076-4085. doi:10.1021/am3028537
12. Stolik S, Delgado JA, Perez A, Anasagasti L. Measurement of the penetration depths of red and near infrared light in human "ex vivo" tissues. *J Photochem Photobiol B*. 2000;57(2-3):90-93. doi:10.1016/s1011-1344(00)00082-8
13. Boisselier E, Astruc D. Gold nanoparticles in nanomedicine: preparations, imaging, diagnostics, therapies and toxicity. *Chem Soc Rev*. 2009;38(6):1759-1782. doi:10.1039/b806051g
14. Zwicke GL, Mansoori GA, Jeffery CJ. Utilizing the folate receptor for active targeting of cancer nanotherapeutics. *Nano Rev*. 2012;3. doi:10.3402/nano.v3i0.18496
15. Bahrami B, Mohammadnia-Afrouzi M, Bakhshaei P, et al. Folate-conjugated nanoparticles as a potent therapeutic approach in targeted cancer therapy. *Tumour Biol*. 2015;36(8):5727-5742. doi:10.1007/s13277-015-3706-6
16. Zhong Y, Meng F, Deng C, Zhong Z. Ligand-directed active tumor-targeting polymeric nanoparticles for cancer chemotherapy. *Biomacromolecules*. 2014;15(6):1955-1969. doi:10.1021/bm5003009
17. Monopoli MP, Bombelli FB, Dawson KA. Nanobiotechnology: nanoparticle coronas take shape. *Nat Nanotechnol*. 2011;6(1):11-12. doi:10.1038/nnano.2011.267
18. Monopoli MP, Aberg C, Salvati A, Dawson KA. Biomolecular coronas provide the biological identity of nanosized materials. *Nat Nanotechnol*. 2012;7(12):779-786. doi:10.1038/nnano.2012.207
19. García-Álvarez R, Hadjidemetriou M, Sánchez-Iglesias A, Liz-Marzán LM, Kostarelos K. In vivo formation of protein corona on gold nanoparticles. The effect of their size and shape. *Nanoscale*. 2018;10(3):1256-1264.
20. Zhang X, Zhang J, Zhang F, Yu S. Probing the binding affinity of plasma proteins adsorbed on Au nanoparticles. *Nanoscale*. 2017;9(14):4787-4792.
21. Dobrovolskaia MA, Patri AK, Zheng J, et al. Interaction of colloidal gold nanoparticles with human blood: effects on particle size and analysis of plasma protein binding profiles. *Nanomedicine Nanotechnology, Biol Med*. 2009;5(2):106-117.
22. Tenzer S, Docter D, Kuharev J, et al. Rapid formation of plasma protein corona critically affects nanoparticle pathophysiology. *Nat Nanotechnol*. 2013;8(10):772-781. doi:10.1038/nnano.2013.181
23. Aggarwal P, Hall JB, McLeland CB, Dobrovolskaia MA, McNeil SE. Nanoparticle interaction with plasma proteins as it relates to particle biodistribution, biocompatibility and therapeutic efficacy. *Adv Drug Deliv Rev*. 2009;61(6):428-437.
24. Cedervall T, Lynch I, Lindman S, et al. Understanding the nanoparticle–protein corona using methods to quantify exchange rates and affinities of proteins for nanoparticles. *Proc Natl Acad Sci*. 2007;104(7):2050 LP - 2055. doi:10.1073/pnas.0608582104
25. Goppert TM, Muller RH. Adsorption kinetics of plasma proteins on solid lipid nanoparticles for drug targeting. *Int J Pharm*. 2005;302(1-2):172-186. doi:10.1016/j.ijpharm.2005.06.025
26. Leroux JC, De Jaeghere F, Anner B, Doelker E, Gurny R. An investigation on the role of plasma and serum opsonins on the internalization of biodegradable poly(D,L-lactic acid) nanoparticles by human monocytes. *Life Sci*. 1995;57(7):695-703. doi:10.1016/0024-3205(95)00321-v
27. Camner P, Lundborg M, Lastbom L, Gerde P, Gross N, Jarstrand C. Experimental and calculated parameters on particle phagocytosis by alveolar macrophages. *J Appl Physiol*. 2002;92(6):2608-2616. doi:10.1152/japplphysiol.01067.2001
28. Hadjidemetriou M, Kostarelos K. Nanomedicine: evolution of the nanoparticle corona. *Nat Nanotechnol*.

2017;12(4):288.
29. Whitesides GM. The origins and the future of microfluidics. *Nature*. 2006;442(7101):368-373. doi:10.1038/nature05058
30. Digiacomo L, Palchetti S, Giulimondi F, et al. The biomolecular corona of gold nanoparticles in a controlled microfluidic environment. *Lab Chip*. 2019;19(15):2557-2567.
31. Gref, Luck, Quellec, et al. “Stealth” corona-core nanoparticles surface modified by polyethylene glycol (PEG): influences of the corona (PEG chain length and surface density) and of the core composition on phagocytic uptake and plasma protein adsorption. *Colloids Surf B Biointerfaces*. 2000;18(3-4):301-313. doi:10.1016/s0927-7765(99)00156-3
32. Harris JM. Introduction to biotechnical and biomedical applications of poly (ethylene glycol). In: *Poly (Ethylene Glycol) Chemistry*. Springer; 1992:1-14.
33. Kingshott P, Griesser HJ. Surfaces that resist bioadhesion. *Curr Opin Solid State Mater Sci*. 1999;4(4):403-412.
34. Ogris M, Brunner S, Schüller S, Kircheis R, Wagner E. PEGylated DNA/transferrin–PEI complexes: reduced interaction with blood components, extended circulation in blood and potential for systemic gene delivery. *Gene Ther*. 1999;6(4):595-605.
35. Nikoobakht B, El-Sayed MA. Preparation and growth mechanism of gold nanorods (NRs) using seed-mediated growth method. *Chem Mater*. 2003;15(10):1957-1962.
36. Zhang Z, Jia J, Lai Y, Ma Y, Weng J, Sun L. Conjugating folic acid to gold nanoparticles through glutathione for targeting and detecting cancer cells. *Bioorg Med Chem*. 2010;18(15):5528-5534.
37. BERTEL GARAY, Linda; MENDEZ SANCHEZ, Stelia Carolina y MARTINEZ ORTEGA F. Use in vitro of Gold Nanoparticles Functionalized with Folic Acid as a Photothermal Agent on Treatment of HeLa Cells. *Mex Chem Soc*. 2018;62. doi:http://dx.doi.org/10.29356/jmcs.v62i1.385.
38. Wang M, Fu C, Liu X, Lin Z, Yang N, Yu S. Probing the mechanism of plasma protein adsorption on Au and Ag nanoparticles with FT-IR spectroscopy. *Nanoscale*. 2015;7(37):15191-15196. doi:10.1039/C5NR04498G
39. Fu C, Yang H, Wang M, Xiong H, Yu S. Serum albumin adsorbed on Au nanoparticles: structural changes over time induced by S–Au interaction. *Chem Commun*. 2015;51(17):3634-3636. doi:10.1039/C4CC08372E
40. Deng ZJ, Liang M, Toth I, Monteiro MJ, Minchin RF. Molecular interaction of poly (acrylic acid) gold nanoparticles with human fibrinogen. *ACS Nano*. 2012;6(10):8962-8969.
41. Wang S, Lu W, Tovmachenko O, Rai US, Yu H, Ray PC. Challenge in understanding size and shape dependent toxicity of gold nanomaterials in human skin keratinocytes. *Chem Phys Lett*. 2008;463(1-3):145-149.
42. Vigderman L, Manna P, Zubarev ER. Quantitative replacement of cetyl trimethylammonium bromide by cationic thiol ligands on the surface of gold nanorods and their extremely large uptake by cancer cells. *Angew Chemie Int Ed*. 2012;51(3):636-641.
43. Le Roy C, Wrana JL. Clathrin- and non-clathrin-mediated endocytic regulation of cell signalling. *Nat Rev Mol Cell Biol*. 2005;6(2):112-126. doi:10.1038/nrm1571
44. Scarabelli L, Sánchez-Iglesias A, Pérez-Juste J, Liz-Marzán LM. A “tips and tricks” practical guide to the synthesis of gold nanorods. 2015.